

**RECENT ADVANCES ON EXPERIMENTAL DAM BREACH STUDIES****AVANÇOS RECENTES EM ESTUDOS EXPERIMENTAIS DE EVOLUÇÃO DE BRECHAS EM BARRAGENS**

Sílvia Amaral<sup>1(\*)</sup>, Teresa Alvarez<sup>1,2</sup>, Laura Caldeira<sup>1</sup>, Teresa Viseu<sup>1</sup>, Rui Ferreira<sup>2</sup>

<sup>1</sup>Laboratório Nacional de Engenharia Civil (LNEC), Av. do Brasil, 101, 1700-066 Lisboa, Portugal

<sup>2</sup>CERIS-IST, Instituto Superior Técnico, Universidade de Lisboa, Av. Rovisco Pais 1, 1049-001 Portugal

(\*) [samaral@lnec.pt](mailto:samaral@lnec.pt)

**RESUMO**

*O escoamento decorrente da rotura de uma barragem é um escoamento tridimensional bifásico (composto por água e sedimentos) onde coabitam várias escalas espaciais, pelo que o estudo detalhado do processo de evolução da brecha tem que se apoiar em ensaios experimentais abrangentes e controlados. Visando atingir este objetivo, o presente estudo baseia-se em ensaios experimentais de rotura de barragens de aterro homogéneas com elevado teor de finos (com comportamento mecânico coesivo) realizados numa instalação de média dimensão no Laboratório Nacional de Engenharia Civil (LNEC). Estes ensaios foram realizados em condições hidráulicas e geotécnicas controladas e visaram: i) fornecer regras práticas para a seleção de solos e procedimentos de compactação de aterros para ensaios experimentais de rotura de barragens; ii) desenvolver novas estimativas do hidrograma efluente de barragens em rotura base com base em dados adquiridos localmente; iii) avançar o estado-da-arte no que respeita a compreensão da relação entre a hidrodinâmica do escoamento e a evolução morfológica da brecha durante o processo de rotura por galgamento. De uma maneira geral, consideram-se adequados à realização de ensaios experimentais de rotura de barragens de terra, solos com teores máximos de finos de cerca de 30% compactados por vibração. As novas estimativas do hidrograma efluente da rotura mostraram boa concordância com as estimativas tradicionais, indiciando a necessidade de se estudar detalhadamente o processo de rotura. Estas demonstraram que o caudal efluente da rotura apresenta um aumento gradual, ao invés de um aumento súbito, em resposta ao destacamento “instantâneo” de massas do solo do corpo da barragem. Por fim, deve-se referir-se que os resultados aqui apresentados foram conseguidos através da utilização de instrumentação recente, bem como recorrendo à adoção de métodos de medição inovadores e à utilização de técnicas de análise e pós-processamento de imagem para extração das variáveis de interesse do fenómeno.*

**Palavras-chave:** rotura por galgamento; barragem de terra; processo de evolução de brecha, estimativas do hidrograma efluente da brecha; métodos de análise e pós-processamento de imagem.

**ABSTRACT**

*The flow originated by a dam failure is a complex 3D two-phase flow (water and sediments) where several spatial scales are present and thus the breaching process details can only be addressed with comprehensive and controlled laboratorial work. This study represents a contribution to achieve this goal and is based on laboratory tests with homogenous earthfill dams with high fines content (with a cohesive mechanical behavior), performed in a medium-scale facility at the Portuguese National Laboratory for Civil Engineering. These were performed under hydraulic and geotechnical controlled conditions: i) to provide practical rules for soil selection and procedures for embankment compaction for dam-breach experiments; ii) to develop novel estimates of the breach effluent hydrographs based on local data; and iii) to advance the state-of-the-art in the relation between the*

*flow hydrodynamics and the breach morphologic evolution during the overtopping process. In general, soils within maximum fines content of 30% and compaction by vibration were found adequate for dam breach experiments for the tested soils range. The novel estimates of the breach effluent flow showed good agreement with traditional ones, hence indicating the need to study in the detail the breaching process. The latter demonstrated that the breach effluent flow presents a gradual increase, rather than sudden, in response to the occurrence of soil mass detachments. Finally, it should be mentioned that the results herein achieved were only possible due to the use of recent instrumentation, as well as to the adoption of innovative measuring methods and by extracting the goal variables through image post-processing techniques here presented.*

**Keywords:** *failure by overtopping; earth dam; breaching process; estimates of the breach effluent flow; image analysis and post-processing methods.*

## 1. INTRODUCTION

Dam failures pose significant flood risks to people and property located in the inundated area [1, 2]. The study of embankment dam failures is particularly of interest since this type of dams totalize about 3/4 of the 33105 large dams worldwide (88% being earth dams and 12% rockfill dams [3]) and are, by far, those that fail more frequently. Studies on failure by overtopping of earth dams have particular interest because according to [4] this constitute the primary failure mode of this type of dams (34%).

The first studies on embankment dam failures were of numerical nature being mostly in the last two decades that the laboratorial studies started to arise, typically in small and medium scale facilities [5, 6]. As a result of these studies, several state-of-the-art advances can be pointed out, but there are still several lacks found in literature as, for instance: 1) the definition of a layout for soil selection and embankment construction to perform reliable dam-breach experiments; 2) novel estimates of the breach effluent flow (breach hydrograph), namely based in proximity measurements (data acquired near the breach); 3) detailed studies on the breach morphologic evolution and its relation with the flow hydrodynamics near the breach.

Regarding the first lack what has been observed is that most of the existent experimental studies have been performed by hydraulicians and do not well address the geotechnical issues of the experiments, as the soil selection, the construction procedures and the soil compaction conditions (relative compaction and water content). This work presents a layout for conducting valid the dam-breach experiments (following the same geotechnical

technical criteria required for actual dams) by first presenting the selection process of the earthfill dam soil and second, the compaction method and construction procedure.

Concerning the second lack, although not all experimental studies focus on the same variables, the most commonly studied are the breach geometric evolution and the breach effluent hydrograph (BEH). Regarding BHE estimates, most studies are based on data acquired far from the breach site, therefore they return 'non-local' estimates - usually by applying traditional estimates, as broad-crested weir formulas [7, 8] or by performing a mass balance in the upstream reservoir [9]. However, the 'non-local' character of these estimates may induce filtering of sudden variations on the BEF [10] hiding real flow variations. Studies characterizing both the BEH and the breach geometric evolution [11, 12] demonstrated that the erosive process, in dams composed of soils with high fines content (with a cohesive mechanical behavior), occurs mainly by hydraulic erosion (continuous erosive process) and by occasional occurrence of singular geotechnical failure episodes (GFE), *i.e.* by the detachment of large masses of soil from the dam body, causing sudden increasing of the breach area (discontinuous erosion). From this perspective, it would be expected that the occurrence of GFE would have repercussions on BEH as a local discontinuity (sudden flow increase). However, the studies noted the exact opposite, raising the following question: '*Is the BEH estimated with the traditional methods being well measured?*'

To answer to this question a novel non-intrusive method for estimate locally the BEH, as the product of a velocity normal to a breach cross section and the area of that cross section, was developed under this study. This was based on image analysis to detect the breach boundaries and to calculate the surface velocity field through large-scale particle image velocimetry (LSPIV) [13]. This local estimate of BEH is not affected by the inertial effects existent in the traditional estimates, with only the effects inherent to the adaptation of the flow to the local geometry.

The BEH estimated locally exhibits a continuous temporal evolution similar to the non-local estimates, only without temporal delay. This observation was counterintuitive and motivates the following fundamental research question: *'Why is the BEH continuous when the breach morphological evolution is discontinuous?'*

The answer to this question encompasses the response to the third lack. Hence, a detailed study was carried out in which the flow hydrodynamics and the soil mechanical behavior on the breach were analyzed at a micro-scale, which allowed to investigate the reason why the breach effluent flow remains continuous during the occurrence of GFE.

To accomplish the paper goals an experimental tests program composed of six tests on failure by overtopping of homogeneous earthfill dams were conducted in well-controlled laboratory conditions, in a medium-scale facility located at the Portuguese National Laboratory for Civil Engineering (LNEC), described in §2. The main results of these tests allowed: i) to provide practical rules for soil selection and procedures for embankment compaction for dam-breach experiments; ii) to develop novel estimates of the breach effluent hydrographs (BEH) based on proximity measurements; and iii) to advance the state-of-the-art in the relation between the flow hydrodynamics and the breach morphologic evolution during the overtopping process. The present paper presents these three achievements being that i), ii) and iii) are respectively presented in §3, §4 and §5. It ends with the

presentation of the main conclusions and future suggested work (§6).

## 2. EXPERIMENTAL FACILITY AND MONITORED VARIABLES

The facility used for the experimental tests is a medium-scale facility with the following main geometric dimensions: 31.5 m long; 1.70 to 6.60 m wide; 0.05 to 1.30 m deep (Fig. 1, (a)). Homogeneous earthfill dams with the following main characteristics were adopted (Fig. 1, (b), (c), (d)): 1) heights between 0.45 to 0.48 m; 2) crest lengths of 1.5 m; 3) crest widths of 0.17 m; 4) upstream and downstream slopes of the dam faces of 1V:2H and 1V:2.5H, respectively; 5) with a downstream toe drain for seepage control.

The main results of the experimental tests program were based on measurements of the inflow, water levels at the reservoir and the settling basin, and on high quality images acquired with an image acquisition layout specially assembled for this purpose (composed by 5 different cameras - 2 HD; 2 high-speed; Kinect sensor (RGB and IR camera) and a high power laser sheet). Further details on the facility, the experimental set up, on the image acquisition layout and its components and on the procedure for measuring these parameters can be found in [10] and [13].

## 3. DAM-BREACH EXPERIMENTS: DEFINITION OF PRACTICAL RULES FOR SOIL SELECTION AND EMBANKMENT COMPACTION PROCEDURES

### 3.1 Properties of the soil

The failure by overtopping of homogeneous earthfill dams is a phenomenon where both hydraulic and geotechnical processes are present. Accordingly, the characteristics of the experimental earthfill dams cannot be defined only attending to hydraulic similarity considerations. For instance, experimental earthfill dams scaled from Froude similarity do not necessarily simulate rigorously the shear forces and the erosive phenomena. In fact, when performing dam-breach experiments two problems usually arise:

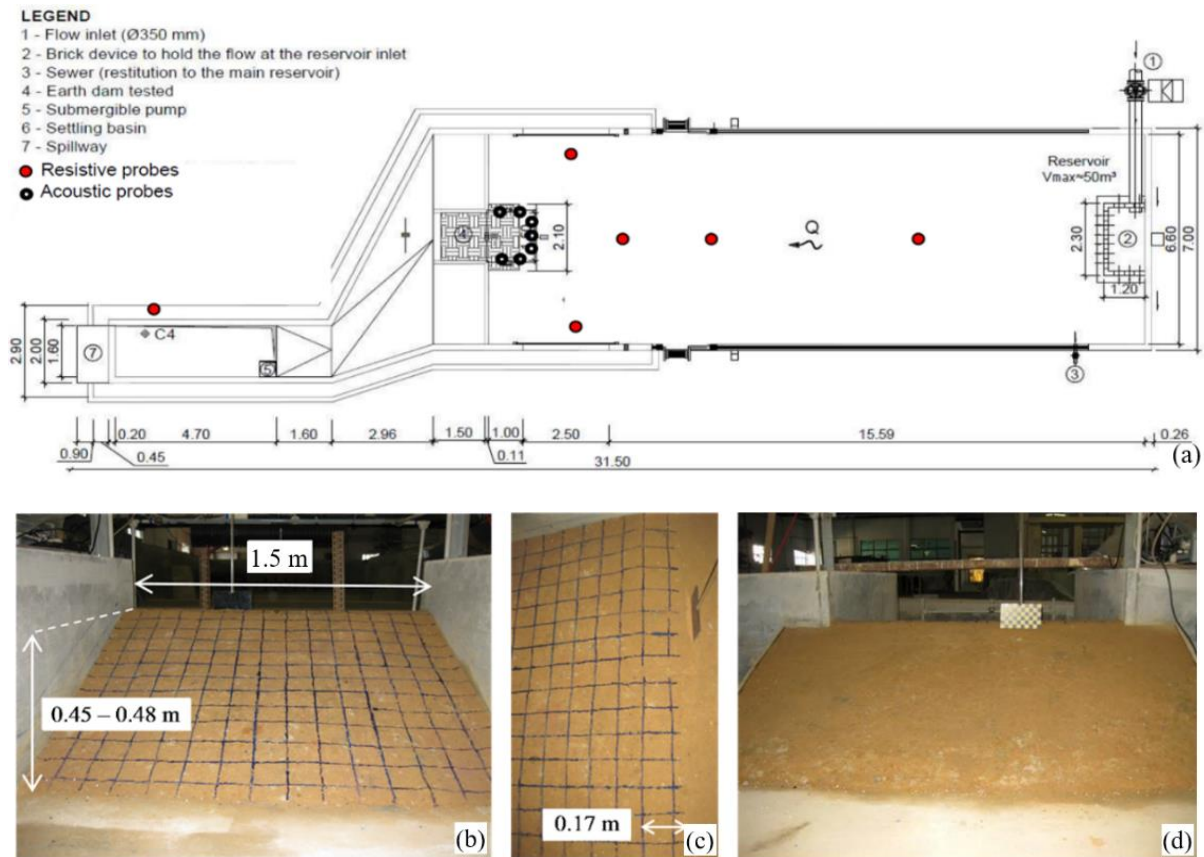


**Fig. 1** - (a) Plan view of the experimental facility (dimensions in meters); Homogeneous embankment dam model: (b) downstream slope; (c) top view, with the crest width; (d) upstream slope

- 1- do not necessarily simulate rigorously the shear forces and the erosive phenomena. In fact, when performing dam-breach experiments two problems usually arise:
- 2- a grain size distribution curve geometrically scaled would represent a soil with physical and mechanical properties completely different from those of the prototype, and ultimately with a different superficial erosion behaviour (soil with higher fines content – with lower permeability and shear strength and higher deformability and erosion resistance);
- 3- the velocity fields in physical facilities are usually far lower from those of the prototype, and therefore, the shear stresses applied superficially by the flow in the former are smaller than those on the latter.

In respect to the first problem, the grain-size distribution curve does not necessarily have to be scaled, and in most cases, the soil of the prototype can be used in the experimental tests (further details can be found in [13]). Nevertheless, considering the

second problem, the erodibility in the experimental earthfill dam has to be increased to overcome the fact that, in laboratory, the shear stresses applied by the overtopping flow will be much smaller. This was achieved experimentally by reducing the relative compaction and testing different water content scenarios in the experiments (creating earthfill dams less resistant to erosion) when compared with real dam practice. The following guidelines were followed:

- relative compactions (RC) varying from 80 to 90% of the standard Proctor reference values were considered a good trade between an embankment that still maintains realistic geotechnical behaviour and presents the erodibility characteristics compatibles with the purpose;
- two different scenarios of water content deviations from the reference value determined from the standard Proctor test ( $w_{optimum}$ ) were studied:

- $w \in w_{optimum} \pm 2\%$  (usual reference interval);
- $w < w_{optimum} - 2\%$  (below the usual lower limit, *i.e.* to aggravate the erosion susceptibility).

Although the experimental tests were not performed with soil from any particular homogenous earthfill dam, it was carefully selected. The grain-size distribution curves of several Portuguese homogenous earthfill dams were analyzed allowing to define a range of grain-size distribution curves, typical of this type of Portuguese dams that served as a base for selecting the soil to be used in experimental tests (Fig. 2 (a)), grey zone). The upper limit of this range is a silty sand (SM) or a clayey sand (SC) with gravel and the lower limit is a lean clay (CL<sup>1</sup>) according to the USCS [14] (Fig. 2 (a)).

Among several samples of sand, silty and clayey soils, as well as of natural soils, whose grain-size distribution curves were determined by sieving and sedimentation analysis [15] a natural soil (from a quarry

extraction deposit) and a clay-sand mixture (1:2 – clay:sand) fallen within the goal range (Fig. 2 (b)). The natural soil and the clay-sand mixture are a silty sand (SM) and a clayed sand (SC) - [14] - with 27% and 37% of fines content (Table 1), respectively, therefore, among the intended interval [12-50%]. Both present sufficient low permeability for the purpose ( $\sim 10^{-7}$  m/s – Table 1). Although the natural soil sorts out of the defined range in a small zone it can still be considered representative of a real homogeneous earthfill dams. The clay-sand mixture was used only once (preliminary test) because of its characteristics of instability internal (gap-graded soil).

The grading properties and the corresponding Atterberg limits ( $w_P$ ,  $w_L$ , IP), particles density (G) and coefficient of permeability (k) of the used soils, can be found in Table 1. These parameters were obtained according to [16–18].

The index of erosion rate and critical shear stress at the optimum point of compaction from the Hole Erosion

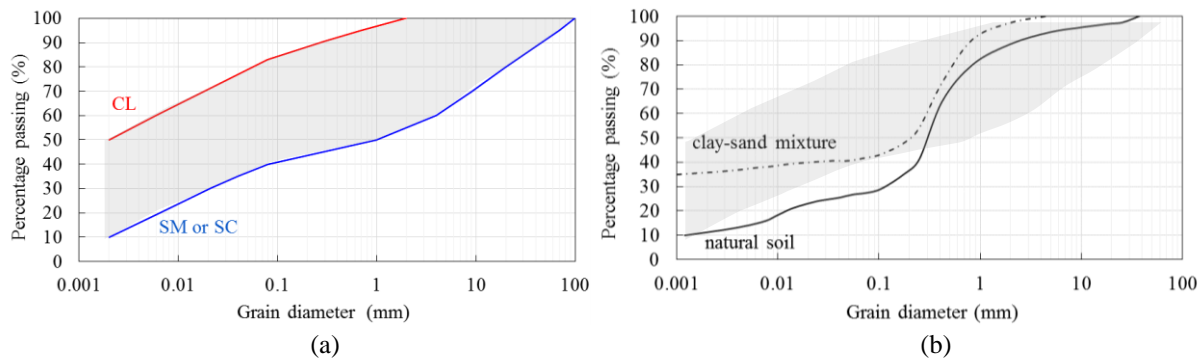


**Fig. 2** - (a) range of grain-size distribution curves that fall under the type of those concerning Portuguese homogeneous earthfill dams; (b) Grain size distribution curves: clay-sand mixture - dashed line; natural soil - continuous line; (grey shade area) target range of grading curves

**Table 1** - Tested soils. Grading properties, Atterberg limits, density and permeability coefficient

Samples	ATTERBERG LIMITS (%)			G (-)	k (m/s)
	$w_P$	$w_L$	IP		
<i>clay-sand mixture</i> $D_{50}=0.23\text{mm}$ ; 37% fines; 61% sand; % gravel	16.5	34.8	18.2	2.67	$6 \times 10^{-10}$
<i>natural soil</i> $D_{50}=0.31\text{mm}$ ; 27% fines; 66% sand; 7% gravel	-	17.5	Non-plastic	2.64	$1 \times 10^{-7}$

$w_P$  - Plastic limit;  $w_L$  - Liquid limit; IP - Plasticity index; G - Particles density;

k - coefficient of permeability;  $\gamma_d^{\max}$  - maximum dry unit weight;  $w_{optimum}$  - optimum water content

<sup>1</sup> Note that the lower limit of this range has necessarily to be lean clay (low plasticity) because in embankment

dam's fat clays (highly plastic) must be excluded due to their highly expansive and deformable behaviour.

the Hole Erosion Test - HET<sup>2</sup> ( $I_{HET}$  and  $\tau_{HET}$  - [19, 20]) of the *natural soil*<sup>3</sup> were respectively 4.0, and 36.7 N/m<sup>2</sup>, which qualitatively corresponds to a soil with a “moderately rapid” rate of progression of internal erosion.

### 3.2 Earthfill dams construction

The compaction conditions affect the physical and mechanical properties of embankments and hence a suitable compaction control during the construction is required.

The study of the compaction conditions to adopt in the experimental tests program was performed: 1<sup>st</sup>) by first determining the reference compaction conditions from the standard Proctor test [22] for the used soil (natural soil -  $\gamma_d^{max}=19.9$  kN/m<sup>3</sup>;  $w_{optimum}=9.4\%$ ); 2<sup>nd</sup>) by testing several conditions of the earthfill material (relative compaction and water content) as well as the methods to obtain these conditions (compaction method).

The compaction homogeneity of the experimental earthfill dams was ensured by adopting a multiple lift system (lifts of 5-8 cm thick) in their construction and by controlling the unit weight and water content from samples collected in each lift.

Three different compaction methods were tested (Fig. 3): 1) using a lawn roller filled with water without vibration; 2) by percussion, using a metallic hand tamper; 3)

by vibration, using a low weight vibratory plate (50 kg). The natural soil was used for this purpose.

First method (*lawn roller filled with water with no vibration*) was unable to compact the soil in depth, being hence, discarded. The evaluation of the other two compaction methods was performed by assessing the physical conditions of the soil after compaction for three different compaction efforts, materialized in terms of number of blows (4, 8 and 12) or passages (1, 3 and 6), respectively for the compaction by percussion or vibration. The standard Proctor compaction curve (natural soil), together with the dry unit weights ( $\gamma_d$ ) and water content ( $w$ ) corresponding to the evaluated compaction efforts for each compaction method, percussion and vibratory, are respectively presented in Fig. 4, (a) and (b).

Fig. 4 shows that relative compactations within the goal range of relative compactations [80-90%] can be obtained with both tested methods: a) percussional – for all the tested compaction efforts (4, 8 and 12 blows) at the optimum water content ( $w_{optimum}$ ); b) vibrational – for 1 or 3 passes of the vibratory plate at dry conditions ( $w < w_{optimum}$ ), although a single pass would not assure an homogenous embankment. The compaction by percussion also shown to be inefficient when compared with the vibratory compaction.

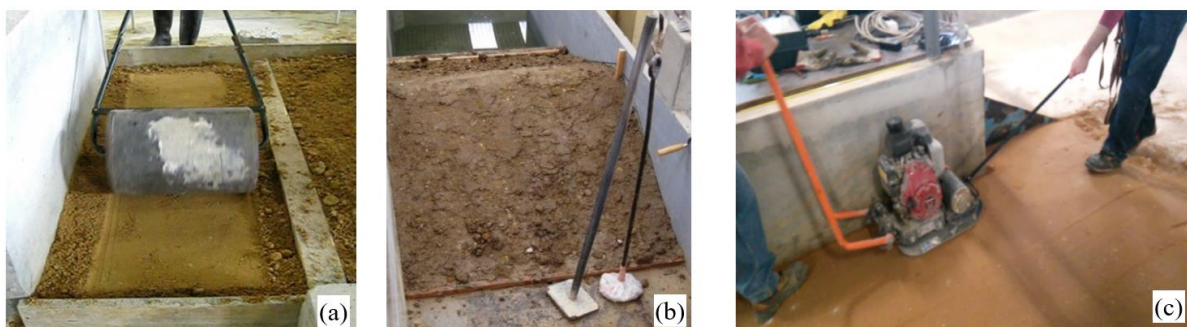
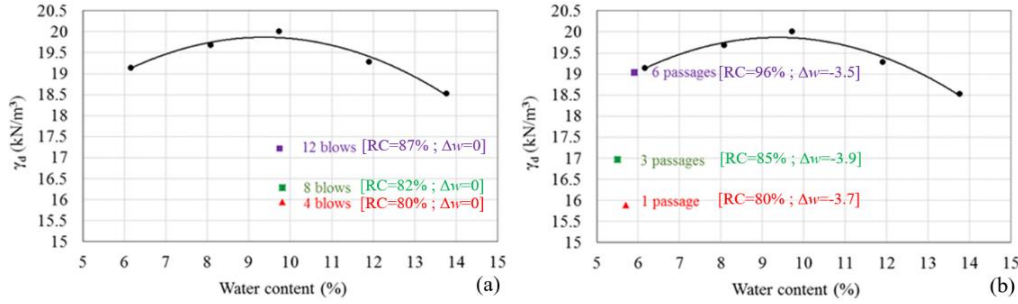


Fig. 3 - Compaction methods evaluated. (a) lawn roller; (b) metallic hand tamper; (c) vibratory plate.

<sup>2</sup> Although the goal of this test is to evaluate the internal erodibility of the soil (important for internal erosion) and the piping progression is quite different from that associated to overtopping failure, the particles detachment process is similar. In fact, several studies have empirical

expressions that relate these erodibilities (internal and superficial).

<sup>3</sup>The HET was not performed for the *clay sand-mixture* because it is not possible to be performed for gap-graded soils was not performed.



**Fig. 4** - Physical conditions of the soil after compaction: (a) by percussions (4, 8, and 12 blows); (b) by vibration (1, 3 and 6 passes)

## 4 NOVEL METHODS TO ESTIMATE BREACH EFFLUENT HYDROGRAPHS

### 4.1 Framework

The discharge,  $Q$ , on any breach cross section whose area is  $A$ , is

$$Q(x_0, t) = \int_{A(x_0, t)} \mathbf{u}(x, y, z, t) \cdot \mathbf{n}(x, y, z) dS \quad (1)$$

where  $x_0$  = coordinate of the centroid of the cross section in an axis that runs down the pilot channel;  $\mathbf{u}$  = velocity distribution at that breach cross section;  $\mathbf{n}$  = unit normal vector pointing out of the reservoir;  $x, y, z$  = three orthogonal spatial coordinates that map the cross section into  $\mathbb{R}^3$ ; and  $t$  = time. Because the flow is unsteady and non-uniform, both the cross section area and the discharge are functions of time and of the specific location  $x_0$  where they are evaluated. At a given instant, there is thus a distribution  $Q(x)$  down the breach, and at a given location, both  $A(x_0; t)$  and  $Q(x_0; t)$  evolve in time. For a given conventional  $x_0$ ,  $Q(x)$  is defined as the breach hydrograph. Accordingly, the breach hydrograph estimate based on Eq. (1) is determined as the product of a velocity normal to the breach cross section ( $\mathbf{u}\mathbf{n}$ ) and the area of that cross section ( $A_{breach}$ ), both characterized in this work by non-intrusive methods based on image analysis detection.

Two different approaches were used to estimate the breach flow area (A and B – §4.3) and the flow velocity field was obtained by large-scale particle image velocimetry (LSPIV – §4.4).

### 4.2 Required equipment and adopted layout

To characterize the variables required to apply this method a laser sheet (Fig. 5 (a), (b)), styrofoam particles distributed on the

flow surface and two high-speed video cameras, one placed upstream the dam monitoring the breach area evolution (Photonfocus – Fig. 5, (c), (d)) and other placed on the top of the dam monitoring the breach geometric evolution from the top and the styrofoam particles displacement across time (Mikrotron – Fig. 5, (e), (f)) properly placed as sketch in Fig. 6.

### 4.3 Breach area estimate

In the present method, the cross sections are vertical because they were obtained with the help of a laser sheet, which was projected vertically (further details can be found in [10]). Two methods – Approach A and Approach B – are proposed for the evaluation of the cross-section area:

- Approach A: The cross section is simply the intersection of the plane of the laser sheet with the submerged dam body and with the free surface; the area  $A(t)$  is that of the plane region encompassed by the traces of the laser sheet in the free surface and in the submerged dam body; the most convenient location to generate this cross section is just upstream the initial dam crest. Fig. 7, (a) shows this definition;
- Approach B: This approach assumes the existence of a curved breach crest line whose elevation is nearly constant – a rim, almost circular, that separates the undisturbed dam body and the incline that leads to the breach channel. Such morphological structure would have been shaped by hydraulic erosion and was indeed observed by [21] (in a non-cohesive embankment) and [9]. The similarity between the breach plan view with the inlet of a culvert was noticed by [22],

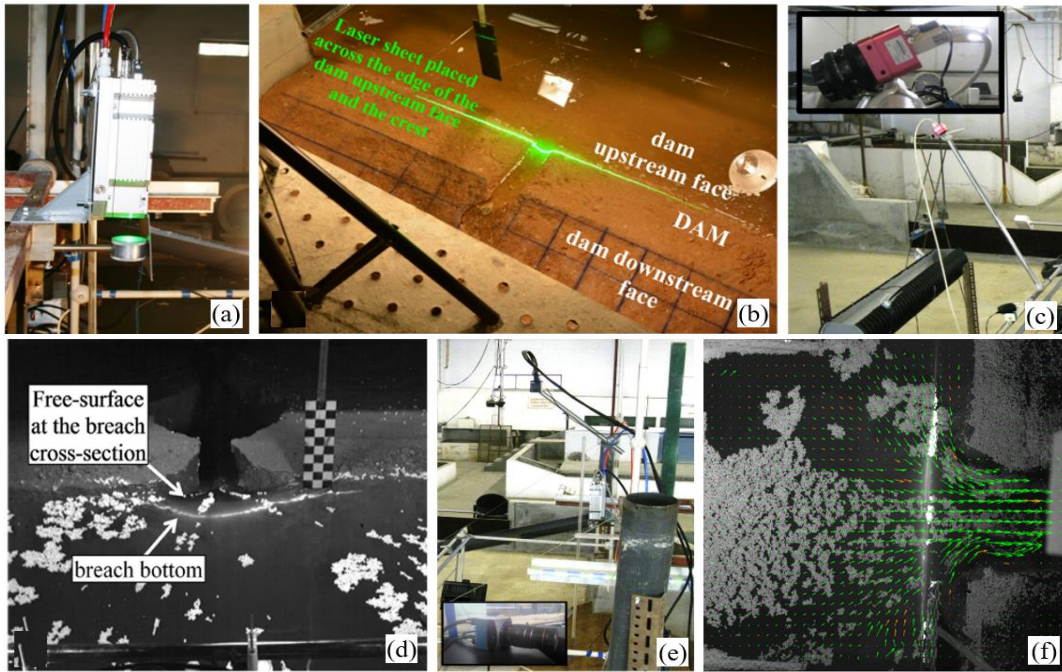


**Fig. 5** - (a) High-power laser coupled to a cylindrical lens for laser sheet creation; (b) illustration of the laser sheet projected in the breach reference section; (c) Photonfocus - upstream high-speed camera positioning; (d) example of an image acquired with the Photonfocus; (e) Mikrotron - top high-speed camera positioning; (f) example of an image acquired with Mikrotron with the representation of the surface velocity vectors from the LSPIV analysis

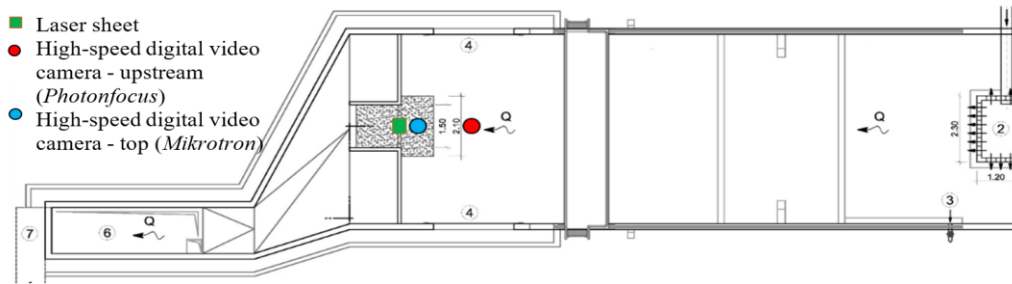


**Fig. 6** - Position of the equipment required for the data acquisition

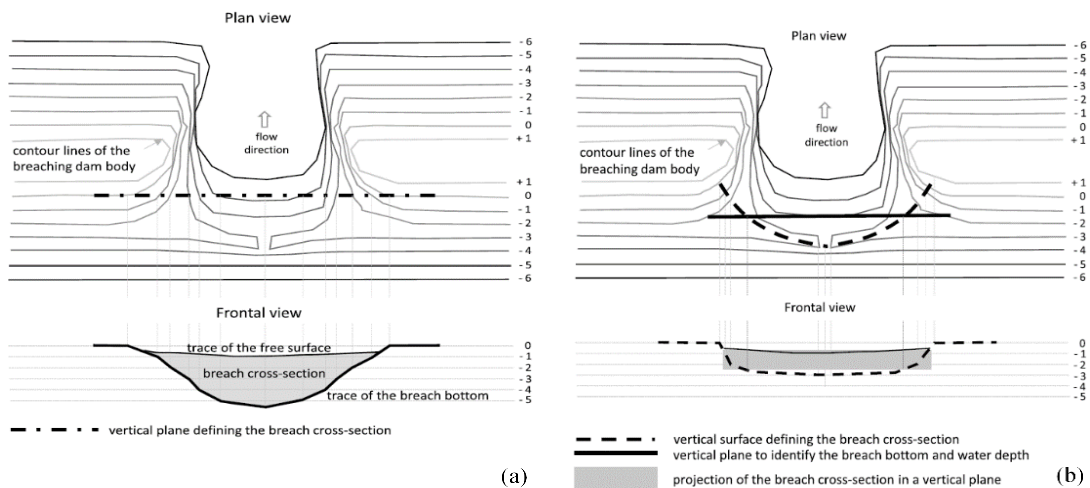


**Fig. 7** - Definition of the breach cross section area. (a) Approach A; (b) Approach B

over which, on a steady flow, the Froude number would be near 1 (critical flow). Assuming that this submerged crest line has

indeed a nearly constant elevation, as represented Fig. 7, (b) as dashed line, its value can be retrieved by the intersection of

a vertical plane (the plane of the laser sheet in this case) with the dam body, as also sketched in Fig. 7, (b) The water depth would be determined by a similar reasoning.

Further details on the image post-processing methods adopted to extract the breach flow area from the images acquired with the high-speed cameras, namely through the Approaches A and B, can be found in [10, 13].

#### 4.4 Flow velocity field estimate through Large Scale Particle Image Velocimetry - LSPIV

The LSPIV method is a non-intrusive remote sensing technique based on image analysis used for flow velocity measurements in a wide range of flow conditions [23]. If the flow is properly provided with 'seeding' (styrofoam particles), *i.e.* with enough quantity uniformly distributed, the LSPIV is a good choice because it causes no disturbances on the flow and allows an adequate spatial resolution of the velocity vectors. This was the method used in the characterization of the surface velocity fields in the near the breach in this work.

The LSPIV base images (acquired with the top high-speed camera - Mikrotron) were filtered for quality enhancement, namely for contrast heightening, noise reduction and peak removal [24]. The filtered images were the base for the estimation of the surface velocity maps with the free-use software PIVlab [25] following the main steps illustrated in Table 2.

The velocity maps in metric units were obtained by using the following calibration process of the base images (Fig. 8, (a) - (c)): 1) placing a chess plate of known dimensions (6x6cm cells) at several dam heights (from the base to the crest) before the test; 2)

reconstructing the flow surface position inside the control volume over time (Fig. 8, (d)) to contemplate the distance variations between the camera and the water surface and allowing to relate the images acquired in a given time with the calibration image placed at the corresponding height. This step 2 was carried out considering the water level data on the breach, extracted through post-processing methods of the images acquired with the upstream high-speed camera (Photonfocus) and the water levels data acquired with seven level probes positioned around the breach.

Fig. 9 shows an example of a velocity map calculation using an LSPIV approach. It illustrates the base images with the definition of the calculation domain (Fig. 9, (a)), the velocity map calculated with PIVlab software, with exclusion of low seeded areas or with high light reflections (Fig. 9, (b)) and the final velocity map converted to metric units after calibration and interpolation processes (Fig. 9, (c)). The mean velocity to consider in the determination of BEH the by the application of Eq (1) corresponds to the mean value of the velocity vectors perpendicular to the breach definition line from approaches A and B (transverse area and radial area, respectively).

#### 4.5 Results and comparison with the traditional estimates of the BEH

The traditional estimates of the BEH (black and grey continuous lines - Fig. 10) and the local ones, developed under this study (Approaches A and B, black, thick and thin lines, respectively - Fig. 10). The red dashed line marks the time of occurrence of one geotechnical failure episode (GFE).

Fig. 10 demonstrates the existence of con-

**Table 2** - Main steps of a LSPIV analysis. PIVlab software.

Input	Images pre-processing	Image Evaluation	Pós-processamento
images from the high-speed video camera Mikrotron	<b>high-pass filter</b> (cut-off=150px)	multiple passes of a Direct Fourier Transform ( <b>DFT</b> ) on an adaptive grid (128x128 → 64x64 → 32x32 px - overlap 50% [linear window deformation])  subpixel resolution to determine the coordinates of the peak - Gaussian interpolation in two orthogonal directions	<b>velocity vectors validation:</b> i) establishing velocity limits; ii) applying a standard-deviation filter  <b>velocity vectors interpolating:</b> elimination of spurious vectors and substitution through interpolation based on valid neighbours  <b>velocity vectors smoothing:</b> application of a smoothing algorithm based on penalized least squares method

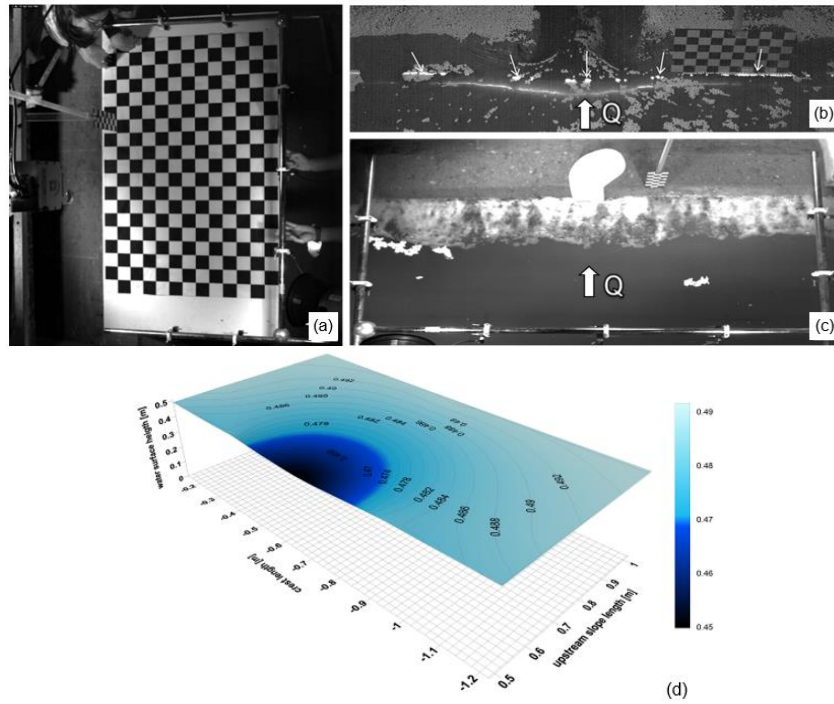


**Fig. 8** - Calibration of the LSPIV base images. (a) calibration plate; (b) water levels on the breach; (c) level probes position around the breach; (d) water surface inside the control volume (dark blue area represents the breach site)

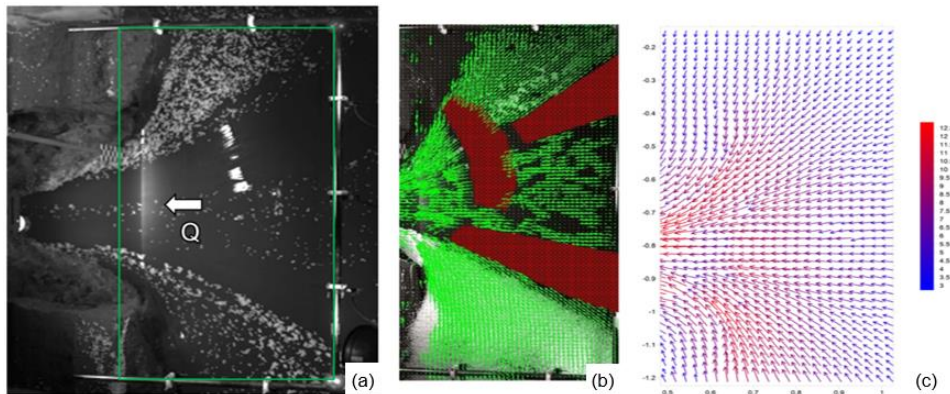


**Fig. 9** - Example of a LSPIV application. (a) definition of the calculation domain (green line); (b) calculated velocity vectors; (c) final velocity vectors (post calibration and interpolation)

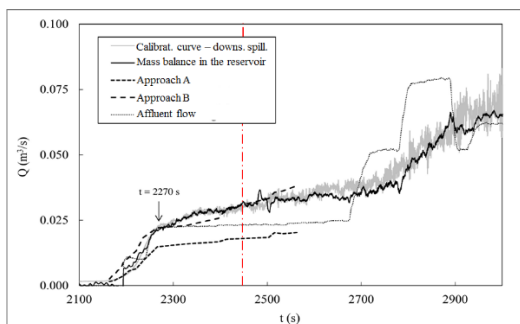


**Fig. 10** - Estimates of the BEH. Traditional and local estimates (A e B). Red dot-trace line – occurrence of a GFE

sistency between the local estimates, A and B, and a similar progress between the later and the 'non-local' estimates (traditional

ones). In particular, the approach B is in agreement with the 'non-local' estimates, both in terms of progression and absolute values. This agreement attributes validity to the local estimates of the BEH developed under this study.

Both 'non-local' (traditional) and 'local' (approaches A and B) estimates were consistent in what concerns the flow behaviours during the GFE, *i.e.* demonstrated a continuous progression. This shows that the breach effluent flow is being well measured since it was measured in two distinct ways ('non-local' and 'local' estimates) and both showed no occurrences of local flow peaks during the GFE. Accordingly, the continuity of the BEH is not a

simplification of the traditional estimates, but rather a fact: a discontinuous erosion does not cause discontinuities in flow (*i.e.*, sudden peaks).

## 5 STATE-OF-THE-ART: ADVANCES IN THE CHARACTERIZATION OF THE FLOW HYDRODYNAMICS AND GEOTECHNICAL PHENOMENA

### 5.1 Monitored variables, measurement forms and additional instrumentation required

In §3 it was shown that the breach effluent flow is being well estimated and that the breach discontinuous erosion, due to GFE, do not induce discontinuities in the flow (sudden peaks). As this observation is counterintuitive, it raises the question: *'If BEH is being well measured, why the discontinuous erosions do not originate flow discontinuities?'*. The present §5 answers to this question.

The monitored variables were:

1. geometry of the contracted flow (width of the non-separated flow - black dashed line in Fig. 11 - measured on the laser sheet);
2. kinematic field next to the GFE (velocity vectors at specific locations – next to the falling blocks – estimated through Particle Tracking Velocimetry (PTV));

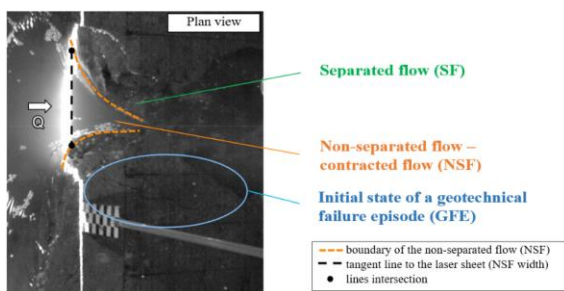


**Fig. 11** - Flow structure and morphology of the channel over the breach

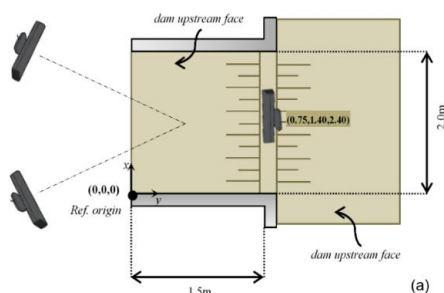


**Fig. 12** - Kinect sensor layout (a) focal positions adopted in the area scanning; (b) position of the targets with known coordinates

- 3 GFE location, dimension, and cause of occurrence → characterization of the erosion below the breach (Fig. 11).

The velocity fields from the LSPIV analysis presented in §4.4, were found appropriate for BEF estimates purposes (§3), *i.e.* to evaluate the flow tendency (flow velocity in the breach section), but insufficient for the accuracy required for fine analysis, as required in this §5. Thus, the velocity field was analysed locally, in carefully selected points next to the GFE, using the Particle tracking Velocimetry (PTV) method. This technique is also a non-intrusive optical method for flow visualization but provides a more detailed view of the particles velocity than that obtained by a PIV cross-correlation analysis. In fact, [26] had already observed that PTV-estimated velocities increased the amount of phenomenological information that could be extracted from a dam breach test.

Beyond the instrumentation presented in §4.2, a Kinect (Microsoft) sensor (motion sensor device, composed of 2 internal cameras - 1 RGB and 1 IR) was added to measure the referred variables. This sensor was used in this study to reconstruct 3D surfaces of the failed dam, namely, to characterize the temporal evolution of the breach morphology. The entire dam scanning was achieved by placing the sensor at three different focal points (Fig. 12, (a)), so that, at least, three target points with known coordinates could be visualized from each sensor position for the purposes of alignment and georeferencing (Fig. 12).

### 5.2 Evaluation of the EEG impact

The evaluation of the GFE impact on breach flow was based on a conceptual model developed under this study that depends on the

GFE location in relation to the position of the hydraulic control section (HCS). Thus, the affectation of the kinematic field and of the width of the non-separated flow was performed according to this conceptual model – Fig. 13.

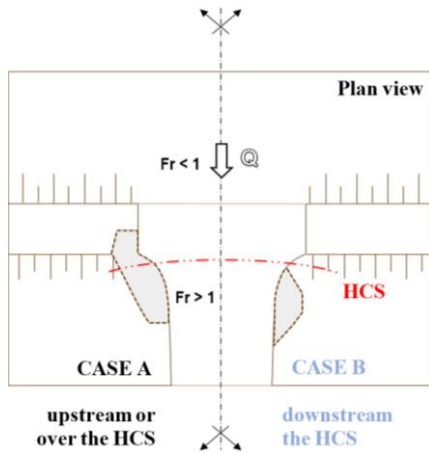


**Fig. 13** - Conceptual model to assess the impact of the GFE on the flow hydrodynamics (kinematic field and width of non-separated flow)

Figs. 14 and 15 illustrate two different situations (Case A and B). For each case, a top image (obtained with the Mikrottron CAV) is presented with the respective location of the velocity calculation areas with PTV (red square in image (a)), the temporal variations of the velocity vectors and the width of the ENS (before, during and after the EEG - vertical dashed in the images (b) and (c), respectively).

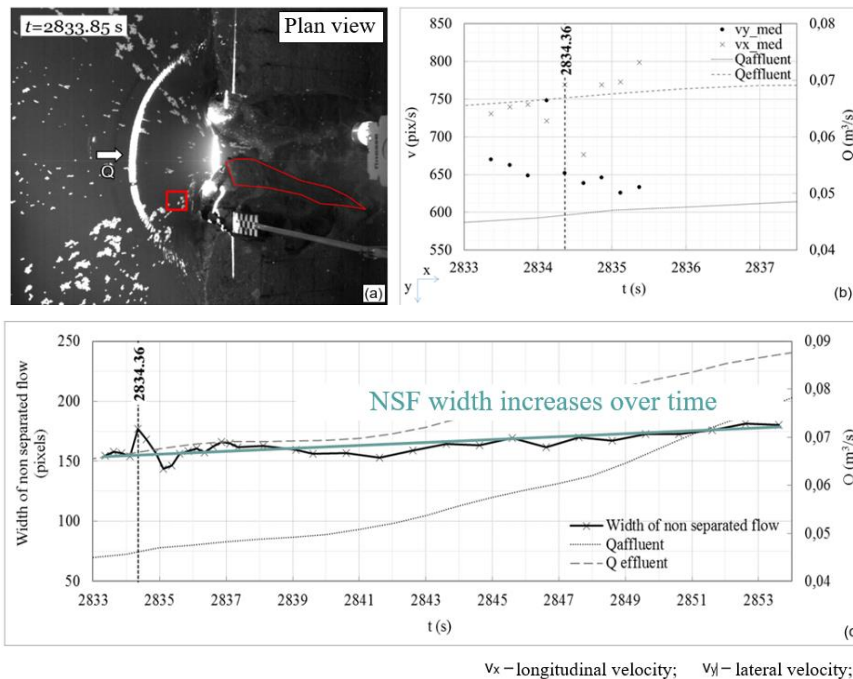


**Fig. 14** - CASE A. GFE impact assessment (a) GFE analyzed with a red square illustrating the area of application of PTV; Temporal variations of: (b) velocity vector inside the red square; (c) NSF width

It was observed that, in Case A, the GFE had an impact on the flow kinematics although the breach effluent flow was not directly affected by the sudden increase on the breach area due to this occurrence (Fig. 14 (b)). In Case B, the longitudinal velocity ( $v_x$ ) did not change and the lateral velocity ( $v_y$ ) suffered only small oscillations that were not associated to the GFE (Fig. 15, (b)). Hence, it was concluded that in this Case B there was no impact on the flow kinematics.

The width variation of the NSF after the occurrence of GFE revealed oscillations in both cases A and B and a gradual increase in Case A (Figs. 14 and 15, (c)). This gradual increase was attributed to a gradual hydraulic erosion of the singularities caused by the GFE.

### 5.3 3D reconstruction of the failed dam with Kinect sensor

As reported in §5.1, Kinect sensor was used in the 3D reconstruction of the failed dam surfaces. Fig. 16, (a) shows a front view of the dam at a failure stage of full development, illustrating the existence of two erosion cavities. Fig. 16 (b) shows a plan view of the points cloud based on the depth images acquired with kinect sensor in all scanning positions (Fig. 12, (a)) and four cross-section proving the existence of these erosion cavities .

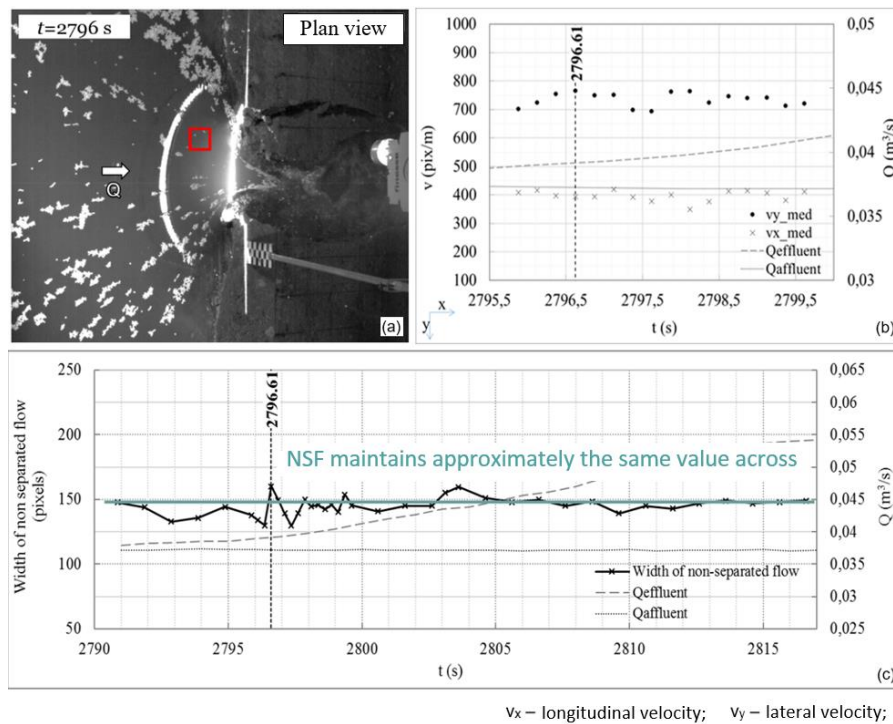


**Fig. 15** - CASE B. GFE impact assessment (a) GFE analyzed with a red square illustrating the area of application of PTV; *Temporal variations of:* (b) velocity vector inside the red square; (c) NSF width

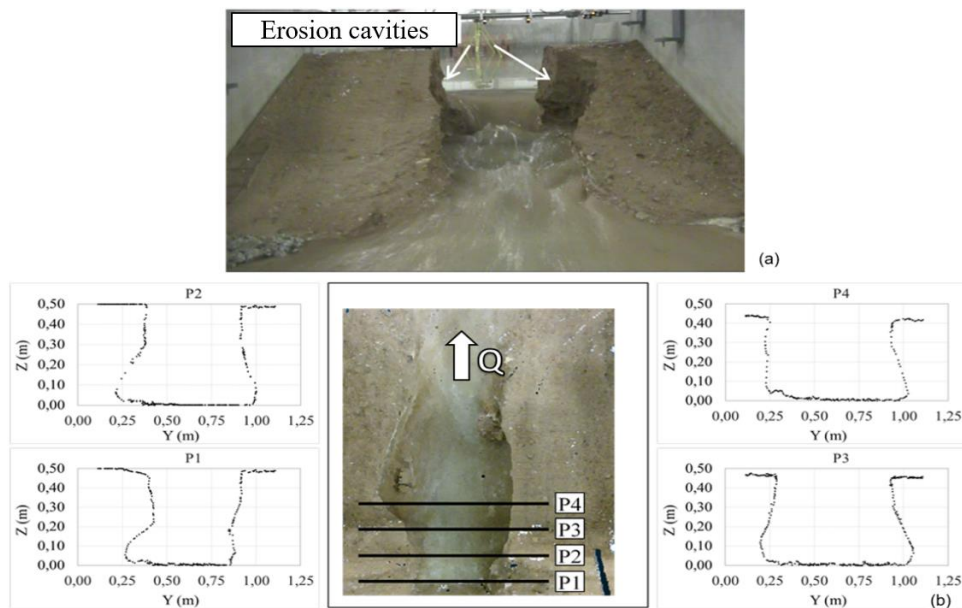


**Fig. 16** - Reconstruction of the failed with the Kinect sensor (a) frontal view of the downstream slope of the dam showing 2 erosion cavities; (b) plan view of the dam (points cloud) with the representation of cross-sections P1 to P4

The 3D reconstruction of the failed dam showed that the failure evolution of the tested dams was predominantly due to headcut erosion with infra-excavation, with occasional appearance of lateral erosion cavities (Fig. 16), which is in agreement with the breaching process of homogeneous earthfill dams (mostly with high fines content, as the earthfill dams tested in this study).

## 6 CONCLUSIONS AND FUTURE WORK

The conclusion of this study is that both ‘non-local’ (traditional) and ‘local’ (approaches A and B) estimates are reliable methods for measuring the breach effluent flow from a failing dam since they are consistent in terms of both progression and absolute values. As both did not showed instantaneous increases in effluent flow during mass detachments from

the dam body (EEG), it has been proved that discontinuous erosion does not cause discontinuities in flow (sudden peaks). Because it was counterintuitive, we inquired on what motivated this fact.

The relation between the flow hydrodynamics and the breach morphological evolution revealed that EEG occur due to underscouring erosion and that these episodes trigger an oscillatory movement of the contracted flow (ENS) that does not impose sudden increases on the flow because they occur in an zone of the dam crest that does not condition this flow. Hence, the increase mechanism of the flow is always gradual for this type of geotechnical instabilities (EEG) because it occurs by gradual erosion of the singularities caused by the falling of the blocks (hydraulic erosion) and that only, in long term, the flow will fill the potential section opened by these episodes. It follows that it should not be assumed that the breach effluent flow can be described by a discharge law of a spillway ( $Q = CA\sqrt{2gH}$ ) because the breach area is not a merely geometric parameter but rather a parameter indexed to the flow hydrodynamics.

## ACKNOWLEDGMENTS

This work was partially funded by FEDER Project, within the scope of COMPETE Program and by the Portuguese National Funding Agency for Science, Research and Technology (FCT), namely by the Project RECI/ECM-HID/0371/2012 and by the PhD scholarships SFRH/BD /47694/2008 and PD/BD/127801/2016.

## REFERENCES

- [1]-T.L. Wahl (2004) Uncertainty of Predictions of Embankment Dam Breach Parameters. *J Hydraul Eng* 130:389–397
- [2]-S.E. Yochum, L.A. Goertz and P.H. Jones (2008) Case study of the big bay dam failure: accuracy and comparison of breach predictions. *J Hydraul Eng* 134:1285–1293
- [3]-(2003) ICOLD. In: International Commission on Large Dams - Bulletin on Risk Assessment in Dam Safety Management (ICOLD)
- [4]-ASCE Task Committee on Dam/Levee breaching (2011) Earthen embankment breaching. *J Hydraul Eng* 137:1549–1564
- [5]-Y. Zhu, P.J. Visser, J.K. Vrijling and G. Wang (2011) Experimental investigation on breaching of embankments. *Sci China Technol Sci* 54:148–155
- [6]-T. Tingsanchali and C. Chinnarasri (2001) Numerical modelling of dam failure due to flow overtopping. *Hydrol Sci J* 46:113–130
- [7]-L. Schmocker and W.H. Hager (2012) Plane dike-breach due to overtopping: Effects of sediment, dike height and discharge. *J Hydraul Res* 50:576–586
- [8]-S. Van Emelen, Y. Zech, S. Soares-Frazao and others (2015) Breaching in sand embankments: Flow-soil interaction. *La Houille Blanche Rev Int l'eau/international water J* 6:21–28
- [9]-J.A. Feliciano Cestero, J. Imran and M.H. Chaudhry (2015) Experimental investigation of the effects of soil properties on levee breach by overtopping. *J Hydraul Eng* 141:4014085
- [10]-A.M. Bento, S. Amaral, T. Viseu, R. Cardoso and R.M.L. Ferreira (2017) Direct Estimate of the Breach Hydrograph of an Overtopped Earth Dam. *J Hydraul Eng* 143:6017004
- [11]-P.J. Frank (2016) Hydraulics of spatial dike breaches
- [12]-J.S. Walder, R.M. Iverson, J.W. Godt, M. Logan and S.A. Solovitz (2015) Controls on the breach geometry and flood hydrograph during overtopping of noncohesive earthen dams. *Water Resour Res* 51:6701–6724
- [13]-S. Amaral (2017) Experimental characterization of the failure by overtopping of embankment dams. PhD Thesis. Instituto Superior Técnico. Universidade de Lisboa
- [14]-ASTM D2487-11 (2011) Standard Practice for Classification of Soils for Engineering Purposes (Unified Soil Classification System). ASTM Int West Conshohocken, PA

- [15]-Especificação LNEC E 196 (1966) Solos - Análise granulométrica. Laboratório Nacional de Engenharia Civil, Lisboa
- [16]-NP-143 (1969) Solos - Determinação de limites de consistência. Laboratório Nac Eng Civil, Lisboa, Port
- [17]-NP-83 (1965) Solos - Determinação da densidade das partículas. Laboratório Nac Eng Civil, Lisboa, Port
- [18]-ASTM D7664-10 (2010) Standard test method for measurement of hydraulic conductivity of unsaturated soils. Am Soc Test Mater Int
- [19]-C.F. Wan and R. Fell (2004) Laboratory tests on the rate of piping erosion of soils in embankment dams
- [20]-T.L. Wahl and Z. Erdogan (2008) Determining erosion indices of cohesive soils with the hole erosion test and jet erosion test. US Department of Interior, Bureau of Reclamation, Technical Service Center
- [21]-S.E. Coleman, D.P. Andrews and M.G. Webby (2002) Overtopping Breaching of Noncohesive Homogeneous Embankments. *J Hydraul Eng* 128:829–838
- [22]-H. Chanson (2004) *Hydraulics of open channel flow*. Butterworth-Heinemann
- [23]-M. Muste, I. Fujita and A. Hauet (2008) Large-scale particle image velocimetry for measurements in riverine environments. *Water Resour Res* 44:
- [24]-M. Raffel, C.E. Willert, S.T. Wereley and J. Kompenhans (2007) *Physical and Technical Background*. In: *Particle Image Velocimetry*. Springer, pp 15–77
- [25]-W. Thielicke and E. Stamhuis (2014) PIVlab—Towards user-friendly, affordable and accurate digital particle image velocimetry in MATLAB. *J Open Res Softw* 2:
- [26]-B. Orendorff, C.D. Rennie and I. Nistor (2011) Using PTV through an embankment breach channel. *J Hydro-environment Res* 5:277–287